Available online at www.sciencedirect.com

ScienceDirect

Geochimica et Cosmochimica Acta 245 (2019) 304–315

Geochimica et Cosmochimica Acta

www.elsevier.com/locate/gca

X-ray powder diffraction study of the stability of clathrate hydrates in the presence of salts with relevance to the Martian cryosphere

Emmal Safi [a,b,1], Stephen P. Thompson [b], Aneurin Evans [a,*], Sarah J. Day [b] Claire A. Murray [b], Annabelle R. Baker [b], Joana M. Oliveira [a], Jacco Th. van Loon [a]

[a] *Astrophysics Group, Lennard-Jones Laboratories, Keele University, Keele, Staffordshire ST5 5BG, UK*
[b] *Diamond Light Source, Harwell Science and Innovation Campus, Didcot, Oxfordshire OX11 0DE, UK*

Received 26 September 2017; accepted in revised form 31 October 2018; available online 9 November 2018

Abstract

Water on the present day Martian surface is thought to exist in two thermally distinct sub-surface reservoirs: as ice in the cryosphere and as groundwater located deeper in the crust. These sub-surface environments are thought to contain saline, rather than pure, water and laboratory studies on whether or not clathrate hydrates can form in such environments are lacking. We fill this gap by performing synchrotron radiation X-ray powder diffraction to investigate the formation and evolution of clathrate hydrates in weak chloride solutions at CO_2 pressures, and over temperature ranges, that are similar to those found in the Martian regolith. We have found that clathrate hydrates can form under conditions relevant to the Martian cryosphere, despite the presence of chloride salts. We find that the dissociation temperatures for CO_2 clathrate hydrates formed in saline solutions are depressed by 10–20 K relative to those formed in pure water, depending on the nature of the salt and the CO_2 pressure. We suggest that the inhibiting effect that salts such as $MgCl_2$, $CaCl_2$ and NaCl have on clathrate hydrate formation could also be related to the salts' effect on the formation of the low temperature phase of ice. However, despite the inhibiting effect of the salts, we conclude that the presence of clathrate hydrates should still be possible under conditions likely to exist within the Martian cryosphere.

Keywords: Freezing brines; Chlorides; CO_2 clathrate hydrates; X-ray powder diffraction; Martian cryosphere; Mars

1. INTRODUCTION

Clathrate hydrates (hereafter "clathrates") are cage-like structures formed at high pressures ($\gtrsim 0.6$ MPa) and low temperatures ($\lesssim 300$ K) (Sloan and Koh, 2007) in which water molecules, bonded via hydrogen bonds, can encase guest gas phase molecules (Sloan and Koh, 2007). The type of guest molecule that can be trapped within a clathrate determines the clathrate structure, of which three are currently known: sI, sII and sH (see Sloan and Koh, 2007, for a review).

sI clathrates form a cubic structure with space group Pm-3n (see Fig. 1 for the structure of sI, the subject of this paper), and are composed of two cage types: the smaller 5^{12} (12 pentagonal faces) and the larger $5^{12}6^2$ (12 pentagonal faces and 2 hexagonal faces). sI clathrates are constructed of two small cages for every six larger ones, and host relatively large molecules such as CO_2 and CH_4. They have the

* Corresponding author.
E-mail address: a.evans@keele.ac.uk (A. Evans).
[1] Present address: School of Natural and Environmental Sciences, Drummond Building, Newcastle University, Newcastle upon Tyne NE1 7RU, UK.

https://doi.org/10.1016/j.gca.2018.10.034
0016-7037/

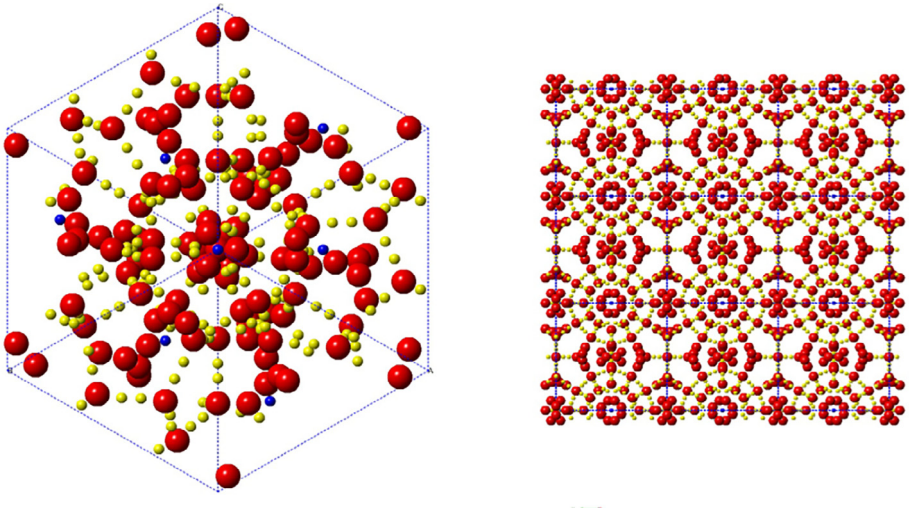

Fig. 1. Structure of CO_2 clathrate. Blue symbols = carbon, yellow = hydrogen, red = oxygen. Left: unit cell viewed along the c axis; right: crystal comprising 3 × 3 unit cells viewed along a axis. Atom positions taken from Henning et al. (2000). (For interpretation of the references to color in this figure legend, the reader is referred to the web version of this article.)

ideal stoichiometry $2M_s{\cdot}6M_l{\cdot}46H_2O$ (where M_s and M_l represent guests in small and large cages, respectively). sII also form cubic structures (space group Fd3m) and are composed of sixteen small 5^{12} cages and eight large $5^{12}6^4$ cages (ideal stoichiometry $16M_s{\cdot}8M_l{\cdot}136H_2O$); sII clathrates typically host smaller molecules such as O_2 and N_2. The least common clathrate hydrate, sH, is composed of one large cage, three smaller cages and two medium $4^35^66^3$ cages. sH clathrates form hexagonal structures (space group P6/mmm; $2M_{s'}{\cdot}3M_s{\cdot}M_l{\cdot}34H_2O$) and usually require two types of guest species in order to remain stable.

Several different experimental methods have been used to study the formation of clathrates at temperatures below the freezing point of water (Kawamura et al., 2002; Kuhs et al., 2006; Falenty et al., 2013; Ambuehl and Elwood Madden, 2014). These studies have shown that clathrates form in two stages. The first is a nucleation stage, in which gas and ice react at the surface of an ice particle and clathrate cages form rapidly. Here the ice particle size controls the rate of formation of the clathrate layer that subsequently surrounds the ice particle (Ambuehl and Elwood Madden, 2014). The second stage is much slower and involves gas and/or water diffusing thru the clathrate shell (Kawamura et al., 2002). In addition, since most studies relate to clathrate formation in pure water/ice, the effect that impurities, such as dissolved salts, have on both clathrate formation and subsequent behavior is not fully understood.

Recently we reported (Safi et al., 2017) on the formation of CO_2 clathrate in the presence of $MgSO_4$, finding that the dissociation temperatures and pressures of CO_2 clathrate are depressed, by as much as 10–20 K over the pressure range 5–20 bar.

In this paper we consider the effects that chlorides can have on both the ice and clathrate phases, and discuss our results in the context of the Martian cryosphere.

2. MARS

2.1. Clathrates on Mars

Early in its history, Mars is believed to have possessed a planetary inventory of water equal to a global equivalent layer ~ 0.5–1 km deep (Carr, 1986, 1996). Although some of the H_2O inventory has been replenished by H_2O exsolution from magmas (Craddock and Greeley, 2009), since the Late Hesperian ~ 15% of the original inventory of H_2O is thought to have been lost to space (Valeille et al., 2010).

Of the water remaining today ~ 90–95% is believed to reside in two thermally distinct sub-surface reservoirs (Carr, 1986, 1996):

(i) as ice in the cryosphere; and
(ii) as groundwater located deeper in the crust, where radiogenic heating is thought to have increased lithospheric temperatures above freezing (Fanale, 1976; Rossbacher and Judson, 1981; Clifford, 1993; Carr, 1996; Clifford and Parker, 2001).

The average thickness of the cryosphere likely varies from 0–9 km at the equator, to ~ 10–22 km at the poles (Clifford et al., 2010).

Within the cryosphere (at depths down to a few kilometers) and in the near sub-surface (depths down to a few meters), conditions are also suitable for the existence of clathrates (Mousis et al., 2013a). The pressure below the present-day Martian surface is dominated by the lithostatic pressure which, assuming the surface is predominantly tholeiitic basalt (McSween et al., 2009), is given by $P_{\mathrm{lith}} \simeq 11\ [h/100\ \mathrm{m}]$ bar at depth h. Had the atmospheric pressure in the past been higher ($\simeq 2$ bar, as suggested by Chassefière et al., 2013) the pressure at depth h would have been correspondingly enhanced in Mars' past such that his-

toric clathrate formation at depth could have extended much deeper than present day conditions might suggest; furthermore, under these conditions, clathrates would have been more stable at shallower depths.

Under present day conditions, the lowest and highest surface temperatures in the south polar region are 150 K and 303 K (Mousis et al., 2013a). Calculations suggest that, under these conditions, CO_2 clathrates should be stable at the coldest temperature and unstable at the highest surface temperature and, therefore, likely to dissociate. In order for Martian clathrates to remain stable throughout the Martian year they would need to be buried at a depth of at least 1.1 m (Mousis et al., 2013a).

The thermodynamic stability field of clathrates on Mars extends to different depths in different regions. According to models, at the equator it reaches to within the top 15 m of the surface and extends to a depth of 3–5 km, while at the poles it reaches the surface and extends down to depths of 8–13 km (Chastain and Chevrier, 2007; Ambuehl and Elwood Madden, 2014). This implies that a large reservoir of CO_2 clathrate is available; such a reservoir could have been enhanced by an early CO_2-rich atmosphere. CO_2 gas is believed to be present in large quantities at depth (Mousis et al., 2013a). In Nature, ice is rarely composed of pure water and will contain volatiles prior to clathrate formation. Ambuehl and Elwood Madden (2014) suggest that the presence of volatiles will affect the clathrate formation and dissociation processes and therefore the ice caps and frozen lakes, or oceans, preserved as permafrost on the planet.

Some geomorphic features on the surface of Mars are attributed to the dissociation of clathrates. For example, certain observed chaotic terrain is the result of a collapsed cratered region due to the removal of surface material that may include clathrates (Baker, 2009). The dissociation of CO_2 clathrates is thought to be one of the causes of floods on the Martian surface (Hoffman, 2000). Understanding the dissociation of clathrates can thus lead to a better understanding of how the release of CO_2 from permafrost and polar caps is influenced by seasonal temperature changes, seismic events, landslides, pore water salinity changes, impacts and changes in obliquity (Ambuehl and Elwood Madden, 2014).

2.2. Salinity of Martian water

Salinity is an important factor to consider in the context of the Martian surface as it depresses the freezing point of water (Sloan and Koh, 2007; Safi et al., 2017). Widespread surface deposits consistent with the presence of chloride-bearing material were detected by the Mars Odyssey Thermal Emission Imaging System (THEMIS; Osterloo et al., 2008). Surface samples collected by landers and rovers at various locations all show similar chlorine concentrations of between 0.2 and 1 wt% (Glavin et al., 2013). In addition, the Sample Analysis at Mars experiment on the Curiosity Rover detected chlorinated hydrocarbons at approximately the temperature at which the rise in O_2 – released from fines sampled at the Rocknest site – was observed (Glavin et al., 2013). The high chloride content of the Martian regolith could be a simple consequence of the fact that chloride salts are highly soluble; it could also be due to the dispersal of early brine, or the wind dispersal of dried evaporite dust (Burt and Knauth, 2003).

Studies on the thermodynamic and chemical stability of salts on Mars have shown NaCl, $MgCl_2$, $CaCl_2$ and LiCl are likely to be present, with the freezing point of the brines being as low as 210 K (Burt and Knauth, 2003; Clifford et al., 2010). In fact $MgCl_2$ and $CaCl_2$ are considered to be the most fitting salts responsible for the Recurring Slope Lineae on the Martian surface (Chevrier and Rivera-Valentin, 2012), which are thought to be due to the transient flow of brines.

Due to the fact that clathrates form at lower temperatures in saline solutions, a shift in the clathrate stability zone will occur. This could potentially change the structure of clathrates by altering the way in which gas molecules occupy the cages (Sloan and Koh, 2007). The presence of clathrates at the base of the Martian cryosphere is thought to be primarily constrained by the low temperatures and pressure at depths close to the base of the cryosphere (Mousis et al., 2013a). Due to their density and fluid nature, brines which occur in the regolith on Mars should lie between an upper ice layer and a lower salt layer (Burt and Knauth, 2003).

Elwood Madden and Bodnar (2002) carried out geochemical thermal modeling to predict the Martian brine composition. They found that a chloride ion brine could be a stable fluid at low temperatures ($\sim$ 250 K), while a sulfate ion brine – at the same temperature – has low solubility leading it to become saturated and precipitate out, leaving chloride as the dominant liquid phase ion.

3. METHODS

In this work aqueous solutions of $MgCl_2$, $CaCl_2$ and NaCl were used to form the ice and CO_2 clathrate system. The concentrations, temperature ranges and pressures used are summarised in Table 1. We have used the minimum concentration of chlorine thought to be present on Mars for our $MgCl_2$ solution ($\sim$0.2%; Glavin et al., 2013; Gough et al., 2016), as this is one of the salts that is present to a lesser extent. Similarly, we have used the maximum concentration of chlorine thought to be present on Mars for our $CaCl_2$ solution ($\sim$1%; Glavin et al., 2013; Gough et al., 2016), due to its possible dominance on the Martian surface. Finally we have used an intermediate concentration of chlorine thought to be present on the Martian surface for our NaCl solution ($\sim$0.6%, Glavin et al., 2013; Gough et al., 2016). The salt concentrations used are the lower, mid and upper values of chlorine detected by landers and rovers in all locations on the Martian surface (Glavin et al., 2013). The temperatures used in this experiment include the range found at Mars' polar ice caps (Falenty et al., 2011) and the pressures used are representative of clathrates forming below the Martian surface.

In the experimental data reported below, we refer to an individual set of data showing either heating or cooling as a "run"; and "cycle" is used to refer to a set of data that has undergone both heating and cooling successively.

Table 1
Concentration, temperature range and pressure of the salt solutions used in this work. Concentrations were chosen to match those found by landers and rovers on the Martian surface (Glavin et al., 2013). See text for choice of temperature and pressure values.

Salt	Concentration g/kg H_2O	Temperature range (±5) (K)	Pressure (bar)
$MgCl_2$	2	90–242	10 ± 0.1
$CaCl_2$	10	90–193	10 ± 0.1
$CaCl_2$	10	200–268	20 ± 0.1
NaCl	6	169–250	10 ± 0.1

In situ Synchrotron X-ray Powder Diffraction (SXRPD) data were collected using the fast position sensitive detector on beamline I11 at the Diamond Light Source (Thompson et al., 2009, 2011), during nine 8-h shifts. The incident X-ray wavelength was 0.825654 Å, calibrated against NIST SRM640c standard Si powder. Details of the high pressure gas cell and the procedures used to form the clathrates have been described previously (Day et al., 2015), while information on the cycling techniques can be found in Safi et al. (2017). In brief, a 0.8 mm diameter single-crystal sapphire capillary is filled with the salt solution and sealed into the gas cell. This is then mounted onto the beamline's concentric three circle diffractometer, and cooled using a liquid nitrogen (LN_2) cryostream which has a temperature stability of ±0.1 K and a ramp rate of 360 K/h. The experimental arrangement is shown in Fig. 2.

Once ice has formed at ~ 240 K, CO_2 gas is admitted to the cell at the selected pressure. The cell contents are then thermally cycled once, leading to the simultaneous formation of clathrate and ice upon subsequent cooling; this "second cycle" technique leads to enhanced and more rapid clathrate formation. The position sensitive detector is used to collect in situ SXRPD data during this process which, in total, takes approximately 20 min. The second cycle technique is described in more detail in Day et al. (2015) and Safi et al. (2017).

For the present work we cycled the temperature between the ranges given in Table 1. Clathrate dissociation temperatures were determined by holding the sample at constant pressure and gradually increasing the temperature in 5 K steps until no clathrate peaks were discernible in the X-ray diffraction pattern: this provides a robust way of determining whether or not clathrates are present. Each SXRPD data-collection cycle, including the time allowed for the sample to come to equilibrium at each temperature step, took approximately 20 min.

In the case of the 10 g $CaCl_2$ solution, the first set of cooling data could not be used due to ice forming on the outside of the cell as a result of slight misalignment; accordingly there are no "Cycle 1, cooling" data for this sample, and the misalignment was corrected at the base temperature. Also, for the NaCl sample, there was a temporary loss of the synchrotron beam which resulted in a relatively large increment in the cooling cycle, which could not be recovered during the beam-time allocation.

The SXRPD patterns were analysed using TOPAS refinement software (Coelho, 2007). During fitting, the lattice parameters of Ih were initially set to 4.497479 Å for the *a*–axis and 7.322382 Å for the *c*–axis (Fortes, 2007); the lattice parameter for Ic was initially set to 6.36 Å and for clathrates to 11.893 Å (Motoi, 1968; Udachin et al., 2001). The space groups of sI clathrate, Ih and Ic are Pm-3n, P63/mmc and Fd3m respectively. From the refinements the percentage of each phase present was determined at

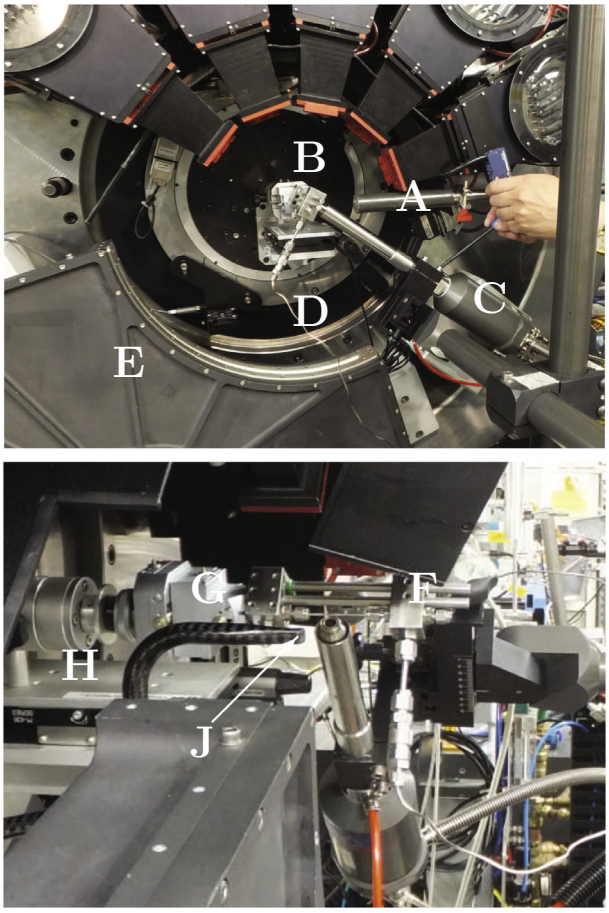

Fig. 2. Gas cell mounted at center of I11 diffractometer. Top, side view: (A) X-ray beam pipe, (B) diffractometer θ-circle, (C) LN_2 cryostream, (D) CO_2 gas delivery line, (E) position sensitive detector. Bottom: view of cell (F) looking towards the X-ray beam, showing cell alignment goniometer (G) mounted on a linear translation stage (H). In this arrangement, the sample capillary is beneath the two bracing struts. Also visible is the beam back stop (J), which is removed in top image. During data collection the capillary is rocked using the θ-circle motor to increase the in-beam sample averaging.

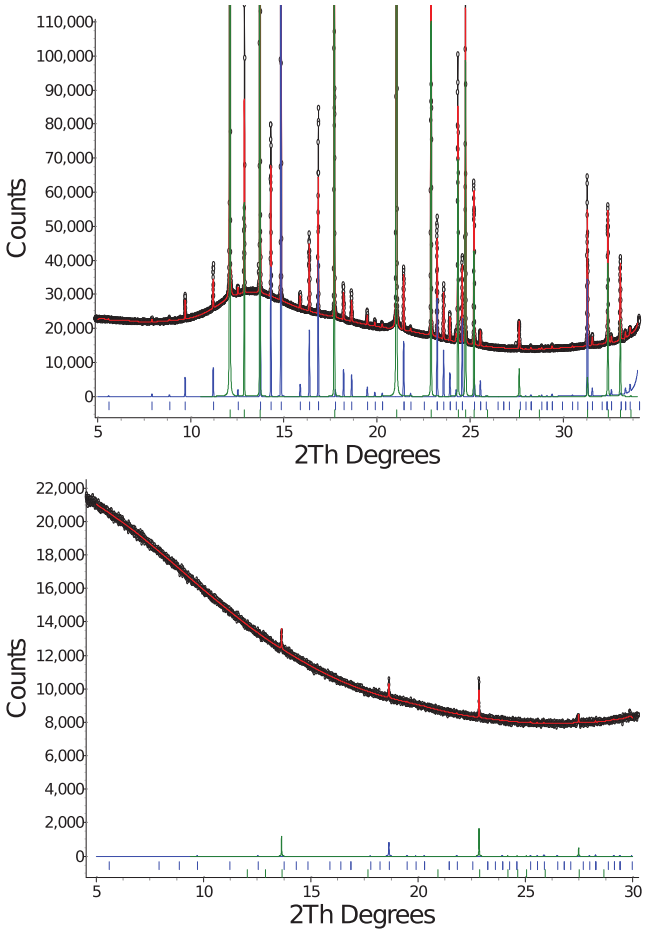

Fig. 3. Top panel: fit (red) to SXRPD data (small circles) at 180 K, showing mixture of ice and clathrates (top trace). Bottom trace shows calculated contribution of each phase to the diffraction pattern; markers below show positions of ice and clathrate features. Note that the intensity scale has been set to truncate the ice peaks in order to show the weaker clathrate peaks. Bottom panel: fit (red) to SXRPD data (small circles) at 290 K just prior to complete clathrate dissociation. Peaks at 13.6°, 22.8° and 27.5° are due to ice, while the single peak at 18.6° is due to vestigial clathrate. (For interpretation of the references to color in this figure legend, the reader is referred to the web version of this article.)

each temperature step during cycling, allowing the formation and dissociation temperatures of clathrates to be established.

A typical example of a refinement is shown in Fig. 3 which shows a comparison of the SXRPD patterns for clathrates, Ih and Ic formed in the $CaCl_2$ salt solution at a CO_2 pressure of 10 bar. We found previously (Safi et al., 2017) that Ic also forms alongside clathrates in the presence of $MgSO_4$ salt solutions, despite being thermodynamically unfavorable. The presence of the clathrates at 90 K and 180 K is evident from the formation of multiple features at 14°–19°, 21.4°, 23–24°, 24.6° and 25.2° 2θ (Day et al., 2015; Safi et al., 2017). Fits to the weaker clathrate peaks were obtained by excluding the ice peaks from the refinement, the values for the weighted profile R_{wp} and background-corrected weighted profile R'_{wp} fitting agreement parameters (see McCusker et al., 1999, for further details) between the calculated and experimental diffraction data for clathrate structures at 90 K and 180 K were $R_{wp} = 6.066\%$ and 4.010% and $R'_{wp} = 21.701\%$ and 19.862% respectively.

4. RESULTS

4.1. Clathrate dissociation temperatures

Table 2 shows the derived clathrate dissociation temperatures. The dissociation temperatures for clathrates formed in the presence of $CaCl_2$ at 10 bar do not differ significantly from those of clathrates formed in the presence of $MgCl_2$, despite the higher concentration of $CaCl_2$ in our experiments. Mg ions in $MgCl_2$ have smaller radii (and therefore higher charge density) than the Ca ions in $CaCl_2$; they are therefore more capable of attracting water molecules (which have high dipole moment). Thus $MgCl_2$ is the stronger inhibitor by comparison with $CaCl_2$ (Sabil, 2009), so that less $MgCl_2$ is needed to produce the same effect as $CaCl_2$.[2] We also note that the dissociation temperature

[2] We note here that the radius of the Cl^- anion is large by comparison with those of any of the cations used here so its inhibiting effect is correspondingly smaller.

Table 2
Clathrate dissociation temperatures (K) during individual runs for the salt solutions indicated.

Pressure (bar)	Cycle 1, heating 10	Cycle 2, heating 10	Cycle 3, heating 20
2 g $MgCl_2$/kg H_2O	247.5 ± 2.5	244.0 ± 2.5	–
10 g $CaCl_2$/kg H_2O	242.5 ± 2.5	246.75 ± 2.5	270.5 ± 2.5
6 g NaCl/kg H_2O	249.7 ± 2.5	252.5 ± 2.5	–

for $CaCl_2$ at a pressure of 20 bar is significantly higher, ~ 270 K, than that at 10 bar, ~ 245 K.

The CO_2 clathrate phase diagram is given in Root and Elwood Madden (2012, see their Fig. 1) for the case of pure water. From this figure, we would expect CO_2 clathrates to dissociate at a temperature of ~ 265 K at 10 bar pressure, and at ~ 280 K at 20 bar. The temperatures in Table 2 are consistently ~ 20 K lower than this at 10 bar ($MgCl_2$, $CaCl_2$, NaCl), and ~ 10 K lower at 20 bar ($CaCl_2$). As discussed by Safi et al. (2017), the presence of salts have a significant impact on the clathrate dissociation temperature. The dissociation temperature for CO_2 clathrates formed in the presence of NaCl may be somewhat higher than for $MgCl_2$ and $CaCl_2$, consistent with the fact that it was the least concentrated solution used in our experiment, but also with its having the least inhibiting ability.

4.2. Weight percentage of clathrate, Ih and Ic ice

From the relative contribution of each phase to the overall scattered intensity in the SXRPD pattern, we can obtain the relative fraction by weight of each crystalline component present in the sample under study. These are shown in Figs. 4–6 as a function of temperature for the 10 g $CaCl_2$ solution at 10 and 20 bar CO_2, the 2 g $MgCl_2$ solution at 10 bar CO_2, and the 6 g NaCl solution at 10 bar CO_2 respectively and discussed in turn below.

4.2.1. 10 g $CaCl_2$ solution at 10 and 20 bar CO_2

The 10 g $CaCl_2$ solution was thermally cycled two and a half times, with data analysis starting at ~175 K, beginning with heating. Fig. 4 shows that, in Cycle 1, heating, no clathrate formed at first, the dominant phase being Ih. As the temperature increased the weight percent (wt%) of clathrate increased, while Ih decreased. At the end of heating in this cycle the relative fractions by weight of clathrate, Ih and Ic were approximately 40%, 55% and 5% respectively. At the end of Cycle 1, heating, the clathrates dissociated at 240 K, at which point data collection was terminated; thereafter, the sample was fast-cooled[3] until clathrates were again observed (at ~ 200 K) and data collection resumed. Consequently the clathrate abundance at the start of Cycle 2, cooling, was close to 100%, as optimal temperatures for ice formation are not reached until 190–180 K, at which temperature the clathrate abundance starts to decline (see Fig. 4). During the remainder of Cycle 2, and Cycle 3, cooling, this percentage varied, with the percentage of Ih fluctuating between 40% and 75% and clathrate between 20% and 60%; the amount of Ic, after Cycle 1, heating, remained at essentially 0%.

In Cycle 3, heating, the relative fraction of each crystalline component continued to follow the same trend; however after reaching ~200 K the percentage of clathrate rapidly rose to 100% when 20 bar CO_2 pressure was applied, while Ih simultaneously decreased until none remained; during this time the percentage of Ic peaked at approximately 10%. This behavior could not be investigated further due to the end of the beamtime allocation.

4.2.2. 2 g $MgCl_2$ solution at 10 bar CO_2

Fig. 5 shows the relative fraction by weight of each component formed in the presence of the 2 g $MgCl_2$ solution. Cooling for this solution started at ~ 220 K; the sample underwent two cycles, where clathrates were initially the dominant phase and continued to increase. Once ~ 180 K was reached Ih became the dominant phase. During Cycle 1, cooling, the fraction of Ic remained close to zero. In Cycle 1, heating, we found that Ih continued to dominate (~ 60 wt %), while clathrate remained at 40 wt%; again the fraction of Ic was negligible. This continued until approximately 230 K, where the fraction of Ih and clathrate were comparable.

During Cycle 2, cooling, clathrate once again was the dominant phase (100 wt%). This remained the case until the temperature reached ~ 170 K, at which point Ih and Ic formed; these became the dominant phases, each contributing approximately 40 wt%, the clathrates now contributing the remaining 20%. This relative fraction by weight for each crystalline component remained the same during Cycle 2, heating.

It is evident in Figs. 4 and 5 (e.g. $MgCl_2$, Cycle 1, cooling and $CaCl_2$, Cycle 2, cooling) that there seems to be a transition between ice Ih and clathrate at temperature ~ 185 K. Interestingly, *for pure water, with no high pressure gas,* it has been known that ice Ic transforms rapidly to ice Ih at temperatures above 180–200 K, although there is also evidence that Ic can remain stable up to 228 K (see e.g. Raza et al., 2011, for a discussion).

In our case however the transition seems to be from *clathrate* (rather than ice Ic) to Ih. During $CaCl_2$ Cycle 2, cooling, on the assumption that there is a rapid transition to ice Ih at ~ 185 K, we might expect the amount of clathrates to decrease as soon as Ih forms. For $MgCl_2$, Cycle 1, cooling begins with increasing clathrate abundance and decreasing Ih; the latter may have been present in relatively small quantities due to the presence of the salt depressing its freezing point. However once 185 K – the optimum temperature for the formation of Ih – is reached, the relative amount of Ih increases. During $MgCl_2$ Cycle 2, cooling, the cycle begins with 100% clathrate, but just below 180 K, the formation of Ih is favoured leading to a decrease in the amount of clathrate. Interestingly, an equivalent transition does not seem to occur for NaCl (see Fig. 6).

4.2.3. 6 g NaCl solution at 10 bar CO_2

Fig. 6 shows the relative fraction by weight of each crystalline component formed in the presence of the NaCl solu-

[3] In this mode the LN_2 cryostream sets the flow rate at the maximum value so that the temperature heads towards its set point at the fastest rate, over-riding the programmed rate.

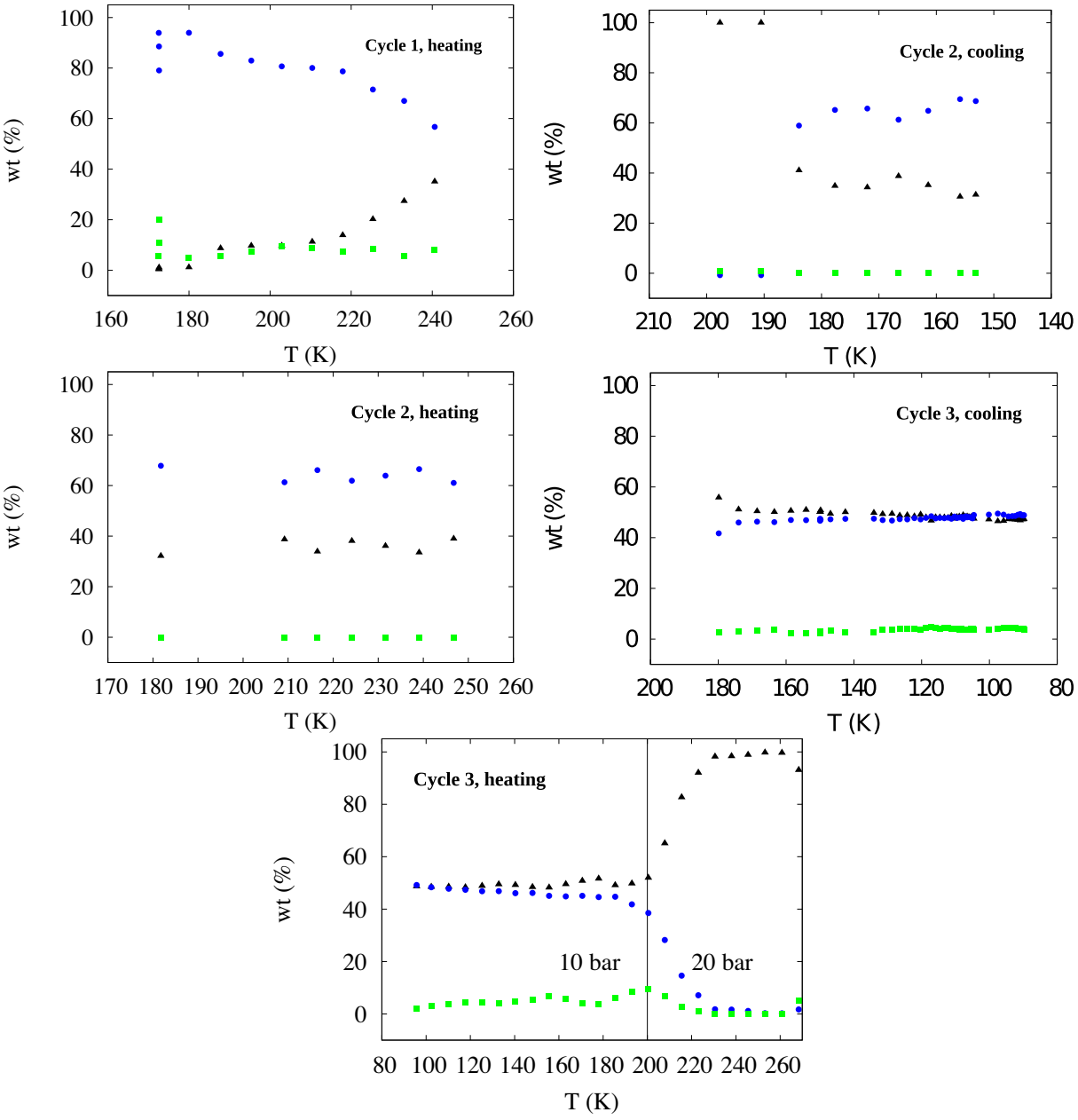

Fig. 4. Relative fraction by weight of clathrates formed in the presence of 10 g $CaCl_2$ solution at 10 and 20 bar CO_2 pressure. Heating and cooling cycles as indicated. Note that there is no "Cycle 1, cooling" for reasons described in text. The apparent jump in clathrate wt% between Cycle 1, heating, and Cycle 2, cooling, is due to the dissociation of clathrates at ~ 240 K and fast-cooling to produce ice at the beginning of Cycle 2, cooling. Vertical line in "Cycle 3, heating" panel indicates an increase in the CO_2 pressure from 10 bar to 20 bar. Black triangles: clathrates; blue circles: Ih ice; green squares: Ic ice. See text for details. (For interpretation of the references to color in this figure legend, the reader is referred to the web version of this article.)

tion. This solution also underwent two cycles, beginning with cooling where the only crystalline phase present was clathrate. This continued to be the case down to ~ 170 K. Clathrates also remained the only crystalline phase during Cycle 1, heating, up to ~ 240 K, at which temperature they dissociated.

During Cycle 2, cooling, Ih was the dominant crystalline phase (~ 80 wt%), while clathrates were present at ~ 20 wt %. As the temperature cooled to ~ 170 K, Ih decreased to ~ 70%, while clathrate increased to ~ 30%. During Cycle 2, heating, Ih decreased even further to ~ 60% and clathrate increased to ~ 40%. At ~ 230 K the proportion of clathrate rapidly increased to ~ 80%, while Ih decreased to ~ 20%. During both cycles using NaCl as the salt solution we observed no Ic.

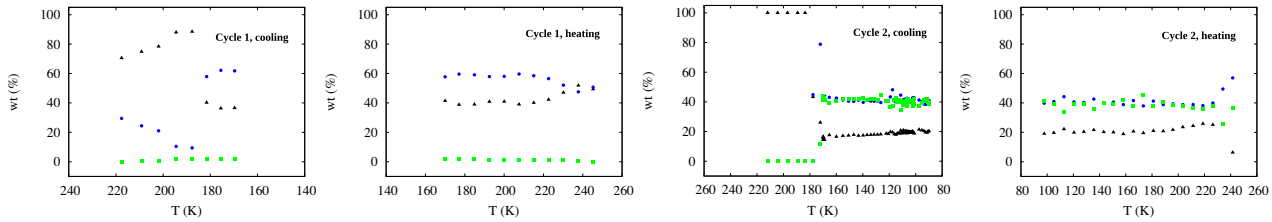

Fig. 5. Relative fraction by weight of clathrates formed in the presence of 2 g $MgCl_2$ solution at 10 bar CO_2 pressure. Cooling and heating cycles as indicated. Symbols/colors as per Fig. 4. See text for details.

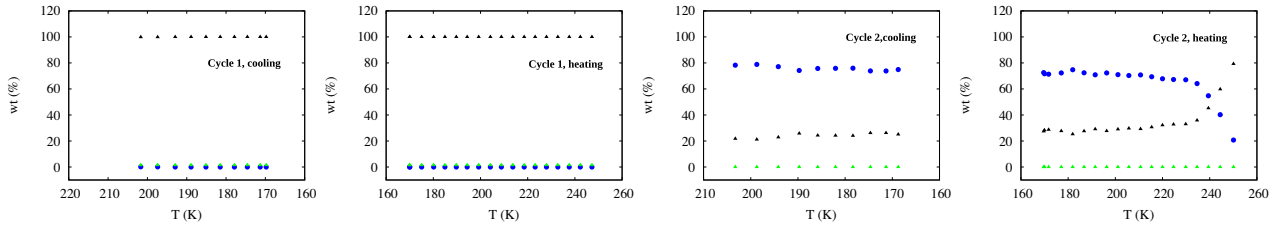

Fig. 6. Relative fraction by weight of clathrates formed in the presence of 6 g NaCl solution at 10 bar CO_2 pressure. Cooling and heating cycles as indicated. Symbols/colors as per Fig. 4. Note the jump from 250 K to 205 K between Cycle 1, heating, and Cycle 2 cooling; this was due to loss of the synchrotron beam, as noted in Section 3. See text for details.

5. DISCUSSION

5.1. The effect of salts

There has been relatively little experimental work on the effect that dissolved salts have on the formation and stability of clathrates, and as mentioned in Section 1, the formation and evolution of clathrates in saline solutions is not well understood.

In this work we have found that the formation of clathrates is possible in conditions that replicate the Martian cryosphere (see Section 2.1), even in the presence of the concentration of salt believed to be present on Mars' surface. We have found that the dissociation temperature for clathrates formed in saline solutions is consistently $\sim$ 20 K lower at 10 bar CO_2 pressure than it is for clathrates formed in pure water. Furthermore, the dissociation temperatures are similar for $MgCl_2$ and $CaCl_2$ despite the concentration of $MgCl_2$ in our samples being lower: this means that weight for weight, Mg is a stronger inhibitor than Ca, for reasons discussed in Section 4.1.

When viewing the clathrate-ice system as a whole, our data also show the salts to have an effect on the ice phase that forms as a result of clathrate dissociation. It is known that the polymorph of ice formed on the surface of a decaying clathrate provides different diffusion pathways for the gas molecule escaping the clathrate cages (Falenty et al., 2011). Ic provides an easier diffusion pathway due to the presence of a large number of grain boundaries and defective zones, hence promoting clathrate dissociation. Ih however, provides a more challenging route and, because it is the thermodynamically more stable phase, Ih inhibits clathrate dissociation (Falenty et al., 2011).

This phenomenon can be seen in Figs. 4–6. During Cycle 1, heating for the $CaCl_2$ solution (Fig. 4), the proportion of Ic is $\sim$ 20% at approximately 170 K, and subsequently decreases as the solution is heated. At $\sim$ 170 K the amount of clathrate increases; this could be a consequence of the decrease in Ic and hence the removal of the easier pathway for clathrate dissociation as the solution is heated, thus allowing clathrates to be more stable in this temperature range. For the remainder of the $CaCl_2$ run, the relative fraction by weight of clathrate remains stable as the proportion of Ic is negligible. During Cycle 3, heating, there is a significant increase in the proportion of clathrates, which can be attributed to raising the CO_2 pressure to 20 bar. Clathrates are more stable at higher pressures (Sloan and Koh, 2007) and raising the pressure by an additional 10 bar in this way results in an increase in the proportion of clathrates produced, independently of the ice phases present.

The behavior of the $MgCl_2$ solution (Fig. 5) can also be attributed to the presence of Ic and its ability to provide an easier pathway for clathrate dissociation. Interestingly, 170 K is $\sim$10 K above the temperature of Ic formation (Falenty et al., 2011). This could imply that the presence of a salt in the solution affects the formation behavior of the ice polymorphs. Mg has a larger inhibiting effect on ice and clathrate compared to Ca (Makogon, 1981, see also above). In this case, as both Mg and Ca ions have the same charge, it is likely to be the smaller size of the Mg that causes it to have a larger inhibiting effect, as discussed in Section 4.1.

Similarly, where there is negligible proportion of Ic present, Fig. 6 shows that, during the experimental run using NaCl as the saline solution, the relative fraction by weight of clathrate does not increase; it is either the dominant phase throughout the entire cycle (as seen in Cycle 1, cooling) or is the dominant phase at the end of the cycle (as seen at the end of Cycle 2, heating).

There are three, possibly related, interpretations of this effect:

1. As discussed by Domin et al. (2016), ice that is formed within the nm-sized pores of mesoporous carbon[4] can display characteristics of both Ic and Ih ice, as we have found here (we note however that Domin et al. (2016) used pure water rather than salt solutions); in our case the confinement is imposed by the clathrate lattice. Domin et al.'s (2016) data suggested the presence of "stacking disordered" ice (Isd) in the pores, and they found that the Ic proportion increases with decreasing pore diameter.
2. Confinement aside, it is possible that (at least part of) the Ih, and the Ic, formed during our experiment are part of a single phase, ice I. Indeed it has been noted that the metastable form of ice I can be made via different routes, including the decomposition of clathrates (Malkin et al., 2015). Ice I is thought to be composed of a combination of cubic and hexagonal stacking sequences and to have a probable trigonal space group P3m1 (Hansen et al., 2008; Kuhs et al., 2012; Malkin et al., 2015) and may be synonymous with Isd; however the hexagonal and cubic stacking probabilities in any specific case are dependent on the formation route (Malkin et al., 2015). It is possible, therefore, that during our clathrate dissociation experiments the low temperature ice phase is better described by ice I, which embodies certain aspects of both Ic and Ih. This would account for the fact that our attempts to identify Ic at 160 K and below were unsuccessful, and could explain why we were seemingly obtaining Ic at an increased freezing point of 170 K.
3. We employed a fast cooling ramp rate of 360 K/h during our experiment such that, potentially, separate Ic and Ih phases may not have been able to form, but rather the formation of a hybrid ice I or Isd phase was driven by the kinetics of fast cooling. Additionally, the ratio of Ih and Ic components in such a phase may vary with temperature (indeed a similar effect was seen by Domin et al., 2016); this could account for the observation of Ic at $\sim$ 170 K during our experiment.

To the best of our knowledge, no experimentally obtained Ic reported in the literature produces a diffraction pattern that is fully representative of the theoretical Fd3m Ic structure (Dowell et al., 1962; Mayer and Hallbrucker, 1987; Kohl et al., 2000; Moore and Molinero, 2011; Malkin et al., 2015). This, unfortunately, means that any diffraction analysis of Ic is limited by the ability of current methods (e.g. Rietveld profile analysis; Hansen et al., 2008) to account for the presence of the hexagonal stacking faults (Murray and Bertram, 2005).

From our current data, we are unable to distinguish between the above hypotheses for the nature and behavior of ice in the presence of clathrates and salts. Stacking disordered ice formation can be considered as a cross-nucleation phenomenon (Yu, 2003, 2007; Chen et al., 2005) between ice polymorphs (Malkin et al., 2015), where one crystal structure nucleates on the face of another, usually favouring the faster growing polymorph, irrespective of whether it is the most stable (Yu, 2007; Nguyen and Molinero, 2014). Indeed, clathrates themselves are the result of cross-nucleation between water crystal polymorphs (Nguyen et al., 2012; Nguyen and Molinero, 2014). Hansen et al. (2008) and Malkin et al. (2015) based their analyses of stacking disordered ice on structural models that incorporated variable numbers of stacking faults, with the latter using bespoke software and very slow cooling rate XRPD data, while the former used standard Rietveld fitting for data obtained by neutron powder diffraction. Hansen et al. (2008) found that, in order to fit their data - collected during the transformation of Ic to Ih - continued addition of ever longer hexagonal stacking sequences to the Ic phase was required, which became computationally intractable. Thus in the absence of a recognised lattice structure for either hybrid ice I or stacking disordered ice (Isd; Domin et al., 2016), we have followed the approach adopted by Hansen et al. (2008) and fitted the data as if the ice consisted of two separate Ih and Ic phases with, in our case, any diffuse scattering contribution from structural disorder taken up by the background function; however we also acknowledge the likely limitations of this approach, and that there is much evidence to suggest our results are likely to be part of a wider and well-documented phenomenon, such that the two phases we have identified may in fact be complementary characteristics of the same hybrid phase.

However, if it is the case that a stacking disordered or ice I phase is the dominant phase whenever clathrates are formed in the presence of chlorides, it may be that this will be the dominant phase of ice present in the Martian cryosphere. Further laboratory work is clearly needed to clarify this point; such work may also offer the prospect of determining suitable observational diagnostics, either remotely, or for data gathering by landers and rovers.

5.2. Implications for the Martian cryosphere

The temperature of the Martian polar and sub-polar surface ranges from 168 to 185 K (Falenty et al., 2011). These temperatures represent the transformation region in the H_2O phase diagram of Ic to Ih. However, it is thought both $CaCl_2$ and $MgCl_2$ (as well as Ca- and Mg- sulfates), along with sodium salts, are present in the Martian polar regions (Knauth and Burt, 2003; Burt and Knauth, 2003; Mousis et al., 2013b). There is some debate as to whether calcium or sodium is the more dominant salt on the Martian surface, depending on whether the salts are chlorides or sulfates. It has been noted that the most stable sulfates on Mars are calcium and magnesium; however due to the fact that the atmosphere is CO_2-dominated, these salts would both be removed as insoluble carbonates (Knauth and Burt, 2003), although some of the calcium may be present as water-soluble calcium perchlorate. This leads to the conclusion that NaCl should be the major soluble salt present in the Martian brines exposed to the atmosphere (Knauth and Burt, 2003). However, Burt and Knauth

[4] A mesoporous material has pores with diameter a few 10s of nm.

(2003) also state that the Martian regolith is basaltic in addition to being significantly reactive. Therefore basalt-brine reactions would have enriched the brine in calcium, with lesser amounts of sodium and magnesium once the brine is isolated from the atmosphere. This implies that partial melting and fractional crystallisation processes could lead to near-surface brines becoming eutectic and highly enriched in $CaCl_2$.

Magnesium is the stronger inhibitor of ice and clathrate, yet we get a large proportion of Ic (and therefore a smaller proportion of clathrate) during our cycles using this as the salt solution. Conversely, when using the weaker inhibitor $CaCl_2$ we obtain a smaller proportion of Ic and a larger proportion of clathrate. As discussed in the previous section, it seems that the type of salt present in the cryosphere of Mars is likely to be an influential factor not only in the formation of clathrates themselves, but also in the phase of ice formed in the presence of clathrates.

It could also be the case that chloride salts are not homogeneously distributed on the Martian surface. This could therefore mean that clathrates in one region could dissociate whilst remaining intact in another. Clathrate dissociation has been suggested as the mechanism behind the formation of seasonal methane plumes observed in various regions of Mars (Mumma et al., 2009). The plumes were observed in three regions over the Northern hemisphere; east of the Arabia Terra, the Nili Fossae region and in the south-east quadrant of the Syrtis Major. Each of these areas shows evidence of ancient ground ice or flowing water. The plumes were seen during the Martian summer and spring, suggesting the permafrost vaporises allowing the methane to escape into the atmosphere. Since methane and carbon dioxide both form cubic sI clathrate structure, these plumes may be caused by the dissociation of clathrates formed in areas of varying chloride content, as they encounter higher temperatures and lower pressures.

In our experiment we cycled the clathrates between approximately 90–270 K. The cycles do not allow us to draw a definitive conclusion on the effect thermal cycling has on the evolution of clathrates. Cycles performed using the $CaCl_2$ and NaCl salt solutions indicate repeated cycling may aid in clathrate formation. However, our results also seem to show that thermal cycling may be detrimental for clathrates formation in the presence of $MgCl_2$.

6. CONCLUSIONS

By the use of in situ SXRPD we have studied the effect that different aqueous chloride solutions have on the formation of clathrates in their presence. Specifically, we have:

1. shown, for the first time, that clathrates can form in the cryosphere of Mars despite the presence of salts;
2. found evidence to suggest that, during the formation of clathrates in our saline solutions, ice I, or ice Isd, may be forming, which embodies structural aspects of both Ih and Ic. This would account for the negligible proportion of Ic even at temperatures of ~90 K where it should be the more stable phase;
3. found that the types of salt (and their inhibiting effect) seems to have a more significant impact on the ice formed, and therefore on clathrate formation, rather than their concentrations.

These experimental observations demonstrate the importance of the role played by salts and, although we have focused on the chloride concentrations typical for Mars, our results may be applicable to other Solar System bodies. Ligier et al. (2016), for example, have suggested that the salts present on the surface of Europa are possibly Mg-chlorides rather than Mg-sulfates. Future experiments focusing on the formation of clathrates and their interaction with various polymorphs of ice in the presence of salt solutions will likely be of fundamental importance to our understanding of other planetary environments.

CONFLICTS OF INTEREST

None.

ACKNOWLEDGEMENTS

This work was supported by the Diamond Light Source thru beamtime award EE9703. ES is supported by Keele University and Diamond Light Source. We thank the reviewers and the Associate Editor for their help in clarifying a number of points in this paper.

APPENDIX A. SUPPLEMENTARY MATERIAL

Supplementary data associated with this article can be found, in the online version, at https://doi.org/10.1016/j.gca.2018.10.034.

REFERENCES

Ambuehl D. and Elwood Madden M. (2014) CO_2 hydrate formation and dissociation rates: application to Mars. *Icarus* **234**, 45–52.

Baker V. R. (2009) The channeled scabland: a retrospective. *Ann. Rev. Earth Planet. Sci.* **37**, 393–411.

Burt D. M. and Knauth L. P. (2003) Electrically conducting, Ca-rich brines, rather than water, expected in the Martian subsurface. *J. Geophys. Res.* **108**, 8026–8031.

Carr M. H. (1986) Mars – a water-rich planet?. *Icarus* **68** 187–216.

Carr M. H. (1996) *Water on Mars*. Oxford Univ. Press, New York, p. 229.

Chassefière E., Dartois E., Herri J.-M., Tian F., Schmidt F., Mousis O. and Lakhlifi A. (2013) CO_2–SO_2 clathrate hydrate formation on early Mars. *Icarus* **223**, 878–891.

Chastain B. K. and Chevrier V. (2007) Methane clathrate hydrates as a potential source for Martian atmospheric methane. *Planet. Space Sci.* **55**, 1246–1256.

Chen S., Xi H. and Yu L. (2005) Cross-nucleation between ROY polymorphs. *J. Am. Chem. Soc.* **127**, 17439–17444.

Chevrier V. F. and Rivera-Valentin E. G. (2012) Formation of recurring slope lineae by liquid brines on present-day Mars. *Geophys. Res. Lett.* **39**, L21202.

Clifford S. M. (1993) A model for the hydrologic and climatic behavior of water on Mars. *J. Geophys. Res.* **98**, 10973–11016.

Clifford S. M. and Parker T. J. (2001) The evolution of the Martian hydrosphere: implications for the fate of a primordial ocean and the current state of the northern plains. *Icarus* **154**, 40–79.

Clifford S. M., Lasue J., Heggy E., Boisson J., McGovern P. and Max M. D. (2010) Depth of the Martian cryosphere: revised estimates and implications for the existence and detection of subpermafrost groundwater. *J. Geophys. Res.* **115**, 7001–7018.

Coelho, A., 2007. TOPAS. General Profile and Structure Analysis Software for Powder Diffraction Data, DIFFRAC plus, Version 4.2 Bruker AXS GmbH:Karlsruhe, Germany.

Craddock R. A. and Greeley R. (2009) Minimum estimates of the amount and timing of gases released into the Martian atmosphere from volcanic eruptions. *Icarus* **204**, 512–526.

Day S. J., Thompson S. P., Evans A. and Parker J. E. (2015) In situ apparatus for the study of clathrate hydrates relevant to solar system bodies using synchrotron X-ray diffraction and Raman spectroscopy. *Astron. Astrophys.* **574**. A91(1–6).

Domin K., Chan K.-Y., Yung H., Gubbins K. E., Jarek M., Sterczynska A. and Sliwinska-Bartkowiak M. (2016) Structure of ice in confinement: water in mesoporous carbons. *J. Chem. Eng. Data* **61**, 4252.

Dowell L. G., Moline S. W. and Rinfret A. P. (1962) A low-temperature X-ray diffraction study of ice structures formed in aqueous gelatin gels. *Biochim. Biophys. Acta* **59**, 158–167.

Elwood Madden M. and Bodnar R. J. (2002) Geochemical modeling of basalt-brine interactions as an analog for Mars near-surface processes. *Lun. Planet. Sci.* **XXXIII**, 1211.

Falenty A., Kuhs W. F. and Hansen T. C. (2011) CO_2 hydrate dissociation at low temperatures – formation and annealing of ice Ic. In *Proceedings of the 7th International Conference on Gas Hydrates*, pp. 17–21.

Falenty A., Salamatin A. N. and Kuhs W. F. (2013) Kinetics of CO_2-hydrate formation from ice powders: data summary and modeling extended to low temperatures. *J. Phys. Chem. C* **117**, 8443–8457.

Fanale F. P. (1976) Martian volatiles – their degassing history and geochemical fate. *Icarus* **28**, 179–202.

Fortes A. D. (2007) Metasomatic clathrate xenoliths as a possible source for the south polar plumes of Enceladus. *Icarus* **191**, 743–748.

Glavin D. P., Freissinet C., Miller K. E., Eigenbrode J. L., Brunner A. E., Buch A., Sutter B., Archer, Jr., P. D., Atreya S. K., Brinckerhoff W. B., Cabane M., Coll P., Conrad P. D., Coscia D., Dworkin J. P., Franz H. B., Grotzinger J. P., Leshin L. A., Martin M. G., McKay C., Ming D. W., Navarro-González R., Pavlov A., Steele A., Summons R. E., Szopa C., Teinturier S. and Mahaffy P. R. (2013) Evidence for perchlorates and the origin of chlorinated hydrocarbons detected by SAM at the Rocknest aeolian deposit in Gale Crater. *J. Geophy. Res. (Planets)* **118**, 1955–1973.

Gough R. V., Chevrier V. F. and Tolbert M. A. (2016) Formation of liquid water at low temperatures via the deliquescence of calcium chloride: implications for Antarctica and Mars. *Planet. Space Sci.* **131**, 79–87.

Hansen T. C., Koza M. M., Linder P. and Kuhs W. F. (2008) Formation and annealing of cubic ice: II. Kinetic study. *J. Phys.: Condens. Matter* **20**, 285105–285118.

Henning R. W., Schultz A. J., Thieu V. and Halpern Y. (2000) Neutron diffraction studies of CO_2 clathrate hydrate: formation from deuterated ice. *J. Chem. Phys. A* **104**, 5066.

Hoffman N. (2000) White Mars: a new model for Mars' surface and atmosphere based on CO_2. *Icarus* **146**, 326–342.

Kawamura T., Komai T., Yamamoto Y., Nagashima K., Ohga K. and Higuchi K. (2002) Growth kinetics of CO_2 hydrate just below melting point of ice. *J. Cyst. Growth* **234**, 220–226.

Knauth L. P. and Burt D. M. (2003) Eutectic Brines on Mars: origin and possible relation to young seepage features. *Icarus* **158**, 267–271.

Kohl I., Mayer E. and Hallbrucker A. (2000) The glassy water-cubic ice system: a comparative study by X-ray diffraction and differential scanning calorimetry. *Phys. Chem. Chem. Phys.* **2**, 1579–1586.

Kuhs W. F., Staykova D. K. and Salamatin A. N. (2006) Formation of methane hydrate from polydisperse ice powders. *J. Phys. Chem. B* **110**, 13283–13295.

Kuhs W. F., Sippel C., Falenty A. and Hansen T. C. (2012) Extent and relevance of stacking disorder in ice Ic. *Proc. Natl. Acad. Sci. U.S.A.* **109**, 21259–21264.

Ligier N., Poulet F., Carter J., Brunetto R. and Gourgeot F. (2016) VLT/SINFONI observations of Europa: new insights into the surface composition. *Astron. J.* **151**, 163–178.

Makogon Y. F. (1981) *Hydrates of Natural Gas*. Penwell Books.

Malkin T. L., Murray B. J., Salzmann C. G., Molinero V., Pickering S. J. and Whale T. F. (2015) Stacking disorder in ice I. *Phys. Chem. Chem. Phys.* **17**, 60–76.

Mayer E. and Hallbrucker A. (1987) Cubic ice from liquid water. *Nature* **325**, 601–602.

McCusker L. B., Von Dreele R. B., Cox D. E., Louë R. D. and Scardi P. (1999) Rietveld refinement guidelines. *J. Appl. Cryst.* **32**, 36–50.

McSween H. Y., Taylor G. J. and Wyatt M. B. (2009) Elemental composition of the Martian crust. *Science* **324**, 736–739.

Moore E. B. and Molinero V. (2011) Is it cubic? Ice crystallization from deeply supercooled water. *Phys. Chem. Chem. Phys.* **13**, 20008–20016.

Motoi K. (1968) Hexagonal and cubic ice at low temperatures. *J. Glaciol.* **7**, 95–108.

Mousis O., Chassefière E., Lasue J., Chevrier V., Elwood Madden M., Lakhlifi A., Lunine J. I., Montmessin F., Picaud S., Schmidt F. and Swindle T. D. (2013a) Volatile trapping in Martian clathrates. *Space Sci. Rev.* **174**, 213–250.

Mousis O., Lakhlifi A., Picaud S., Pasek M. and Chassefière E. (2013b) On the abundances of noble and biologically relevant gases in Lake Vostok, Antarctica. *Astrobiology* **13**, 380–390.

Mumma M. J., Villanueva G. L., Novak R. E., Hewagama T., Bonev B. P., DiSanti M. A., Mandell A. M. and Smith M. D. (2009) Strong release of methane on Mars in northern summer 2003. *Science* **323**, 1041–1045.

Murray B. J. and Bertram A. K. (2005) Formation and stability of cubic ice in water droplets. *Phys. Chem. Chem. Phys.* **8**, 186–192.

Nguyen A. H., Jacobson L. C. and Molinero V. (2012) Structure of the clathrate/solution interface and mechanism of cross-nucleation of clathrate hydrates. *J. Phys. Chem. C* **116**, 19828–19838.

Nguyen A. H. and Molinero V. (2014) Cross-nucleation between clathrate hydrate polymorphs: assessing the role of stability, growth rate, and structure matching. *J. Chem. Phys.* **140**, 084506.

Osterloo M. M., Hamilton V. E., Brandfield J. L., Glotch T. D., Baldridge A. M., Christensen P. R., Tornabene L. L. and Anderson F. S. (2008) Chloride-bearing materials in the southern highlands of Mars. *Science* **319**, 1651–1654.

Raza Z., Alfè D., Salzmann C. G., Klimeš J., Michaelides A. and Slater B. (2011) Proton ordering in cubic ice and hexagonal ice; a potential new ice phase—XIc. *Phys. Chem. Chem. Phys.* **13**, 19788–19795.

Root M. J. and Elwood Madden M. E. (2012) Potential effects of obliquity change on gas hydrate stability zones on Mars. *Icarus* **218**, 534–544.

Rossbacher L. A. and Judson S. (1981) Ground ice on Mars – inventory, distribution, and resulting landforms. *Icarus* **45**, 39–59.

Sabil K. M. (2009) *Phase Behaviour, Thermodynamics and Kinetics of Clathrate Hydrate Systems of Carbon Dioxide in Presence of Thetrahydrofuran and Eletrolytes* (Ph.D. dissertation). Technische Universiteit Delft, Delft, The Netherlands.

Safi E., Thompson S. P., Evans A., Day S. J., Murray C. A., Parker J. E., Baker A. R., Oliveira J. M. and van Loon J. Th. (2017) Properties of CO_2 clathrate hydrates formed in the presence of $MgSO_4$ solutions with implications for icy moons. *Astron. Astrophys.* **600**. A88(1–9).

Sloan E. D. and Koh C. A. (2007) *Clathrate Hydrates of Natural Gas*, second ed. CRC Press, Florida.

Thompson S. P., Parker J. E., Potter J., Hill T. P., Birt A., Cobb T. M., Yuan F. and Tang C. C. (2009) Beamline I11 at Diamond: a new instrument for high resolution powder diffraction. *Rev. Sci. Instrum.* **80**, 75107.

Thompson S. P., Parker J. E., Potter J., Birt A., Yuan F., Fearn R. D., Lennie A. R., Street S. R. and Tang C. C. (2011) Fast X-ray powder diffraction on I11 at Diamond. *J. Synchrotron Radiat.* **18**, 637–648.

Udachin K. A., Ratcliffe C. I. and Ripmeester J. A. (2001) Structure, composition, and thermal expansion of CO_2 hydrate from single crystal X-ray diffraction measurements. *J. Phys. Chem. B* **105**, 4200–4204.

Valeille A., Bougher S. W., Tenishev V., Combi M. R. and Nagy A. F. (2010) Water loss and evolution of the upper atmosphere and exosphere over Martian history. *Icarus* **206**, 28–39.

Yu L. (2003) Nucleation of one polymorph by another. *J. Am. Chem. Soc.* **125**, 6380–6381.

Yu L. (2007) Survival of the fittest polymorph: how fast nucleater can lose to fast grower. *CrystEngComm* **9**, 847–851.

Associate editor: Chris Herd